Generalized Single-Degree-of-Freedom Model to Study Viral Inactivation by Radiated Microwaves

Federica Caselli, Pietro Bia, *Associate Member, IEEE*, Margherita Losardo, Antonio Manna, and Paolo Bisegna

***Abstract*—*Objective*: Recent outbreaks and pandemics have emphasized the need for safe and reliable viral inactivation methods. The purpose of this work is to develop a simple and effective modeling approach to investigate viral inactivation via microwave absorption mediated by dipolar coupling. *Methods:* Leveraging established techniques from the dynamic analysis of structures, a generalized Single-Degree-Of-Freedom (SDOF) model is developed, which is fully consistent with the dipolar resonance mode. *Results:* The model can reproduce the main features of dipolar coupling with minimal computational time. Moreover, it allows mimicking the broadening of the resonance range associated with heterogeneous virus size, via Monte Carlo simulations, as well as water induced damping. *Conclusion:* The results support the potential role of dipolar coupling for viral inactivation by microwave irradiation in the GHz range. The model can be used to assist in the interpretation of the experimental results, leading to an optimization of the inactivation protocols. *Significance:* The proposed approach is versatile and can be extended to describe more complex cases, such as non-spherical geometries and/or non-homogeneous material properties.**

***Index Terms*—Microwave, resonance, dipolar coupling, viral inactivation, generalized SDOF model, numerical simulations.**

I. INTRODUCTION

AIRBORNE pathogens (i.e., disease-causing microorganisms that can be transmitted through the air) represent a serious threat to public health [1]. Notable examples include influenza viruses, which cause the flu, SARS-CoV-2, responsible for COVID-19, and Koch's bacillus, the causative agent of tuberculosis. Airborne pathogens primarily spread through the air when an infected person coughs, sneezes, or talks, releasing tiny droplets that can be inhaled by others. Moreover, they can remain alive on surfaces for varying lengths of time, depending on the type of pathogen, the properties of the surface (e.g., stiffness, porosity), and the environmental conditions (e.g., temperature and humidity). Accordingly, it is crucial to implement disinfection measures to reduce the risk of outbreaks and pandemics. A primary approach is viral inactivation, which refers to any process that renders a virus non-infectious by destroying or disabling its ability to replicate.

Chemical disinfectants are effective against a wide range of microorganisms and are generally available at limited cost. However, some viruses can resist inactivation by chemical agents and certain disinfectants may be toxic to humans and/or harmful to the environment. These limitations have prompted growing interest in safer and more sustainable alternatives [2]. In this context, physical disinfection mechanisms offer valuable opportunities. In particular, virus disruption methods based on irradiation have gained increasing attention in recent years. Although ionizing radiation (such as ultraviolet, X-rays, and gamma rays) is highly effective at inactivating viruses, it poses risks to human health. As a result, non-ionizing radiation approaches, including ultrasounds and microwaves, are preferred. Ultrasound-induced cavitation disrupts viral particles and reduces their infectivity, through mechanical, thermal, and oxidative effects. Microwaves can inactivate viruses through both thermal and non-thermal mechanisms [3], [4], [5], [6]. While thermal effects have been widely used, non-thermal effects are drawing growing interest due to their potential to achieve viral inactivation without relying on elevated temperatures.

Non-thermal microwave viral inactivation may be based on a resonant microwave absorption process that exploits the core-shell charge separation characteristic of viruses [7], [8], [9]. This charge separation enables dipolar coupling between electromagnetic waves and the specific "dipolar" vibration modes of the virus. In particular, viruses are known to resonate in confined-acoustic dipolar modes when exposed to microwaves of matching frequency [7]. The resulting structure-resonant energy transfer (SRET) from electromagnetic waves to the confined acoustic vibrations (CAVs) within the virus can lead to membrane fracture, caused by opposite oscillations of the viral core and shell [10].

Received 1 August 2025; revised 15 October 2025 and 21 November 2025; accepted 17 December 2025. *(Corresponding authors: Federica Caselli; Paolo Bisegna.)*

Federica Caselli and Paolo Bisegna are with the Department of Civil Engineering and Computer Science of the University of Rome Tor Vergata, 00133 Rome, Italy (e-mail: caselli@ing.uniroma2.it; bisegna@uniroma2.it).

Pietro Bia, Margherita Losardo, and Antonio Manna are with Elettronica S.p.A, Italy.

This article has supplementary downloadable material available at https://doi.org/10.1109/TBME.2025.3646706, provided by the authors.

Digital Object Identifier 10.1109/TBME.2025.3646706

Yang et al. [11] investigated SRET from microwaves to influenza A virus and showed higher inactivation ratio of viruses at the dipolar resonant frequency (8.2 GHz). Wang et al. [12] studied microwave absorption spectroscopy of SARS-CoV-2 virus and identified the resonant frequencies of the first and second dipolar modes as 4 and 7.5 GHz, respectively. Considering the pleomorphic properties of SARS-CoV-2, Barbora et al. [13] calculated effective resonant frequencies to be in the 10–17 GHz range. Manna et al. [14], [15], [16] developed an experimental in vitro model to demonstrate SRET-based inactivation of influenza virus and SARS-CoV-2 in aerosols with a microwave power density that is below the limit for safety allowed by worldwide regulatory agencies. The influenza virus was susceptible to higher frequencies, up to 16 GHz, whereas SARS-CoV-2 exhibited sensitivity up to 12 GHz. Moreover, the influenza virus required a longer exposure time (5 minutes versus 1 minute) to attain the same level of inactivation of SARS-CoV-2, under the same experimental conditions. Experimental findings relevant to microwave resonant absorption of viruses and associated viral inactivation are further detailed in Table S1 of the Supplementary Material. Based on the observed frequency-dependence of the inactivation, mechanical fracture induced by resonant dipolar coupling has been pointed out as a possible inactivation mechanism, though viral inactivation was measured via functional assays (plaque assay) rather than direct structural evidence [11], [16].

Notwithstanding the experimental evidence supporting the use of microwaves for safe and effective viral inactivation, a full understanding of the mechanisms involved is yet to be reached. Unraveling those mechanisms would be critical to optimize the inactivation protocols (e.g., frequency range, exposure time, field intensity) depending on the morphological and structural features of the specific pathogen. To this aim, modeling and simulation represent a valuable tool [17]. A common approach to estimate the resonant frequencies of a virus is based on Lamb's theory for the free vibration of an elastic solid sphere [11], [16], [18]. Alternatively, the finite element method (FEM) can be used (e.g., [8], [19], [20]), which allows to account for non-spherical geometries, non-homogeneous elastic properties, and/or different boundary conditions. For instance, Sun et al. [8] investigated resonant dipolar coupling of rod-shaped viruses and performed free-vibration FEM analyses to compare the effect of a capsule shape versus a cylinder on the measured longitudinal mode frequency; Nonn et al. [20] performed FEM-based inverse analysis to determine mechanical properties of SARS-CoV-2 virus from nano-indentation tests according to five different non-homogeneous structural models (i.e., shell models); Warsame et al. [19] performed FEM-based modal analysis of SARS-CoV-2 virus, assuming that the virus is fixed to a host cell by a variable number of spike proteins. Besides versatility, FEM simulations easily provide displacement, strain, and stress distributions within the virus, which is critical to elicit the involved mechanisms. However, this comes at the cost of increased computational time and memory requirements.

The aim of this work is to introduce a modeling approach that is computationally efficient and at the same time fully consistent with the dipolar resonance mode of the pathogen under consideration. Specifically, following an approach commonly used in the dynamic analysis of structures [21], we develop a generalized Single-Degree-Of-Freedom (SDOF) model of the dipolar coupling. Accordingly, the model uses the first dipolar mode of the virus as a shape function. The shape function and the associated model parameters are obtained through FEM-based free vibrations analysis of the pathogen.

The rest of the paper is organized as follows: the basic theory of dipolar coupling is introduced in Section II, the original generalized SDOF model is developed in Section III, simulation results are presented in Section IV, and limitations and perspectives are discussed in Section V.

II. PRINCIPLES OF DIPOLAR COUPLING

Let us consider a homogeneous, isotropic, linear elastic sphere of radius R and denote V_L and V_T as the sound velocities of longitudinal and transverse waves, respectively. The free vibrations of the sphere were studied by Lamb [18] who classified them into torsional and spheroidal modes, further distinguished by their angular momentum number (l) and harmonic index (n). The dipolar active mode corresponds to the spheroidal mode with $l = 1$, and the modes with harmonic indices $n = 0$ and $n = 1$ exhibit significant relative displacement between the core and the shell [7]. As a result, a core-shell charge structure is necessary to enable dipolar coupling in nanoparticles. Due to their inherent charge separation, viruses exhibit such a structure. Liu et al. [7], [9] identified dipolar coupling as the primary mechanism responsible for microwave resonant absorption in spherical viruses, which they modelled as free homogeneous nanoparticles.

According to Lamb's theory, the circular frequency ω of the dipolar modes is obtained by solving the following equation [18]:

$$4\frac{j_2(\xi)}{j_1(\xi)}\xi - \eta^2 + 2\frac{j_2(\eta)}{j_1(\eta)}\eta = 0, \tag{1}$$

where:

$$\xi = \frac{\omega R}{V_L} \quad \eta = \frac{\omega R}{V_T}, \tag{2}$$

and j_1 and j_2 are spherical Bessel functions of the first kind. Equation (1) can be solved numerically (see e.g., [22]). A parametric analysis of dipolar mode eigenfrequency is reported in Section IV-A. As an example, assuming $V_L = 1920$ m/s, $V_T/\,V_L = 1/2$ (i.e., Poisson's ratio equal to 1/3), and $R = 50$ nm, the eigenfrequencies of the first ($n = 0$) and second ($n = 1$) dipolar modes turn out to be 10.99 GHz and 22.13 GHz, respectively. A visualization of those modes, obtained with FEM analysis in COMSOL Multiphysics, is shown in Fig. 1, and animated GIFs are provided as Supplementary Material (Figures S1 and S2). The FEM model is described in Appendix A.

When the frequency of the microwaves matches the natural frequency of the virus's dipolar vibrations, the virus absorbs the microwave energy efficiently. This can cause mechanical stress, possibly leading to the disruption of the viral structure and inactivation of the virus.

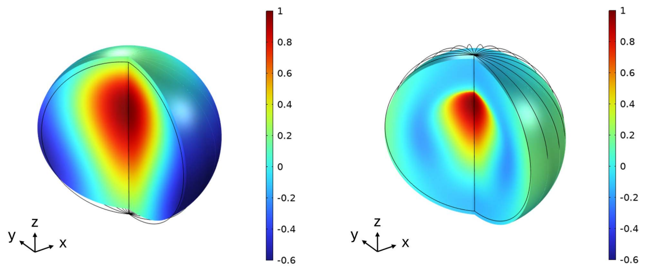

(a) (b)

Fig. 1. Visualization of the z-component ($i.e.,\ w$) of the displacement field of the first (a) and second (b) dipolar mode (arbitrary units).

III. Generalized SDOF Model

Following a continuum-mechanic approach, the equations of motion of an elastic solid subjected to an applied electric field $\boldsymbol{E}$ are given by [23]:

$$\nabla \cdot \left(\mathbb{C} : \hat{\boldsymbol{\nabla}} \boldsymbol{d}\right) + \rho_c \boldsymbol{E} - \rho_m \ddot{\boldsymbol{d}} = 0, \tag{3}$$

where $\boldsymbol{d}$ and $\ddot{\boldsymbol{d}}$ denote the displacement field and its second time derivative (i.e., acceleration), respectively; ρ_c and ρ_m denote charge density and mass density, respectively; $\mathbb{C}$ is the tensor of elastic constants; and the symbols $\hat{\boldsymbol{\nabla}}$ and $\nabla\cdot$ denote symmetric gradient and divergence operators, respectively. Core-shell charge separation is assumed, with uniform charge density within each region. Accordingly, denoting by q the overall charge of the core/shell regions (i.e., $+q$ in the core and $-q$ in the shell), the charge densities are given by $\rho_c^{core} = q/v^{core}$ and $\rho_c^{shell} = -q/v^{shell}$, were v^{core} and v^{shell} denote core volume and shell volume, respectively.

The problem can be recast in the following weak formulation, where $\delta\boldsymbol{d}$ denotes a virtual displacement field and null boundary load is assumed:

$$\int_\Omega \left[\left(\mathbb{C} : \hat{\boldsymbol{\nabla}}\boldsymbol{d}\right)\cdot \hat{\boldsymbol{\nabla}}\left(\delta\boldsymbol{d}\right) + \rho_m \ddot{\boldsymbol{d}}\cdot\delta\boldsymbol{d}\right] d\Omega = \int_\Omega \rho_c \boldsymbol{E}\cdot\delta\boldsymbol{d}\, d\Omega,\ \forall\delta\boldsymbol{d}, \tag{4}$$

where Ω is the region occupied by the virus.

In order to develop the generalized SDOF model, the spatial variation of the displacement field $\boldsymbol{d}$ is assumed to follow that of the first dipolar mode, indicated by $\boldsymbol{\varphi}(\boldsymbol{x})$, with Cartesian components (u, v, w). The time variation is given instead by an unknown scalar function $p(t)$. Thus, $\boldsymbol{d}\left(\boldsymbol{x}, t\right) = \boldsymbol{\varphi}(\boldsymbol{x})p(t)$, $\delta\boldsymbol{d}\left(\boldsymbol{x}\right) = \boldsymbol{\varphi}(\boldsymbol{x})\delta p$ for any scalar δp. The function $\boldsymbol{\varphi}(\boldsymbol{x})$ is normalized such that $w_{poles} - w_{center} = 1$; in this way, $p(t)$ represents the relative vertical displacement between the poles and the center of the sphere.

Accordingly:

$$\left(\int_\Omega \left(\mathbb{C} : \hat{\boldsymbol{\nabla}}\boldsymbol{\varphi}\right)\cdot\hat{\boldsymbol{\nabla}}\boldsymbol{\varphi} d\Omega\right) p\delta p + \left(\int_\Omega \rho_m \boldsymbol{\varphi}\cdot\boldsymbol{\varphi} d\Omega\right)\ddot{p}\delta p = \left(\int_\Omega \rho_c \boldsymbol{E}\cdot\boldsymbol{\varphi} d\Omega\right)\ \delta p,\ \forall\delta p \tag{5}$$

from which, assuming an applied electric field along the unit vector $\hat{\boldsymbol{k}}$ parallel to z:

$$\boldsymbol{E} = \bar{E}\ f\left(t\right)\hat{\boldsymbol{k}}, \tag{6}$$

with $f(t)$ specifying the temporal variation of the electric field, it results:

$$\left(\int_\Omega \left(\mathbb{C} : \hat{\boldsymbol{\nabla}}\boldsymbol{\varphi}\right)\cdot\hat{\boldsymbol{\nabla}}\boldsymbol{\varphi} d\Omega\right) p\delta p + \left(\int_\Omega \rho_m \boldsymbol{\varphi}\cdot\boldsymbol{\varphi} d\Omega\right)\ddot{p}\delta p = \left(\int_\Omega \frac{\rho_c}{q} w d\Omega\right)\ q\bar{E}f\left(t\right)\delta p,\ \forall\delta p. \tag{7}$$

The integral quantities:

$$K = \int_\Omega \left(\mathbb{C} : \hat{\boldsymbol{\nabla}}\boldsymbol{\varphi}\right)\cdot\hat{\boldsymbol{\nabla}}\boldsymbol{\varphi}\, d\Omega, \qquad M = \int_\Omega \rho_m \boldsymbol{\varphi}\cdot\boldsymbol{\varphi}\, d\Omega, \qquad L = \int_\Omega \frac{\rho_c}{q} w\, d\Omega, \tag{8}$$

represent the equivalent stiffness (K), the equivalent mass (M) and the load participation factor (L), respectively.

By exploiting the arbitrariness of δp, and adding a viscous damping term ($C\dot{p}$), (7) leads to:

$$M\ddot{p}\left(t\right) + C\dot{p}\left(\mathrm{t}\right) + Kp\left(t\right) = Lq\bar{E}f\left(t\right). \tag{9}$$

Dividing by M, (9) is recast in the canonical form:

$$\ddot{p}\left(t\right) + 2\zeta\omega_0\dot{p}\left(\mathrm{t}\right) + \omega_0^2 p\left(t\right) = \Gamma q\bar{E}f\left(t\right), \tag{10}$$

with:

$$\omega_0 = \sqrt{\frac{K}{M}}\ \Gamma = \frac{L}{M}\ \zeta = \frac{C}{2M\omega_0} = \frac{1}{2Q}, \tag{11}$$

where $\omega_0 = 2\pi f_0$, with f_0 eigenfrequency of the dipolar mode, Γ normalized load participation factor, ζ damping factor, and Q quality factor. This simple model can be used to perform analyses in both the frequency domain and the time domain. As shown in Sections IV-C to IV-E, it essentially provides the same results as the 3D FEM model with a drastically reduced computational cost.

IV. Results

A. Parametric Analysis of Dipolar Mode Eigenfrequency

According to Lamb's theory (Section II), the eigenfrequencies of an elastic sphere depend on the radius R of the sphere and on the sound velocities of longitudinal and transverse waves (V_L and V_T). Fig. 2 shows the eigenfrequency of the first dipolar mode (i.e., $l = 1, n = 0$) as a function of particle radius R. The latter varies in the range [30, 70] nm, which is characteristic of the SARS-CoV-2 pathogen [24] and includes the range [40, 60] nm typical of influenza virus. In panel A, the velocity ratio is fixed at $V_T/\ V_L = 1/2$, which is a typical value for condensed matter [25], while the longitudinal velocity ranges from 1000 to 2500 m/s. For a 50 nm radius, the eigenfrequency turns out to vary from 5.7 to 14.3 GHz. In panel B, the longitudinal velocity is fixed at $V_L = 1920$ m/s, which was determined for the wet Satellite Tobacco Mosaic Virus (STMV) using Brillouin

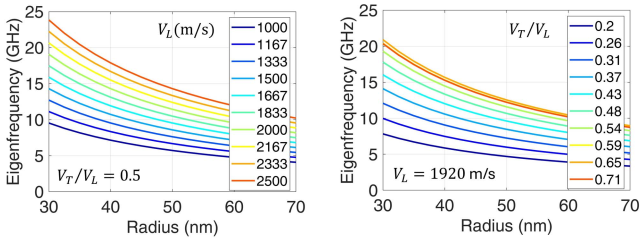

(a) (b)

Fig. 2. Parametric analysis: frequency of the first dipolar mode as a function of particle radius, (a) for fixed velocity ratio and variable longitudinal velocity, and (b) for fixed longitudinal velocity and variable velocity ratio.

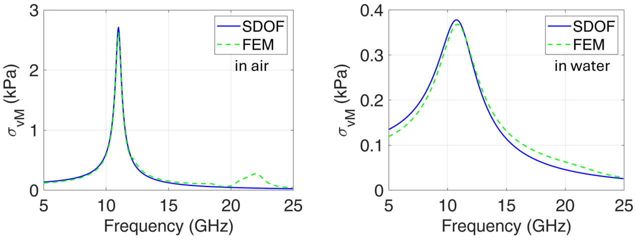

(a) (b)

Fig. 3. Frequency response of a single virus (i.e., Bode amplitude diagram of the von Mises stress σ_{vM}). Comparison of SDOF model and FEM model, (a) in air and (b) in water.

light scattering [25], while the velocity ratio ranges from 0.2 to $1/\sqrt{2}$. The corresponding Poisson's ratios can be found from the relationship [26], [27]:

$$\upsilon = \frac{1}{2}\left(1 - \frac{1}{1/\left(V_T/V_L\right)^2 - 1}\right), \tag{12}$$

and ranges from 0.48 to 0. For a 50 nm radius, the eigenfrequency turns out to vary in the range [4.7, 12.2] GHz, though not monotonically at high velocity ratios.

B. Computation of Generalized SDOF Model Parameters

The parameters of the generalized SDOF model, namely the integral quantities K, M, and L defined in (8), were computed by using the FEM model - Eigenfrequency study (Appendix A). For a 50 nm radius, it turned out: $K = 40.1$ N/m, $M = 8.40 \times 10^{-21}$ kg, and $L = 0.019$. According to (11), a frequency $f_0 = \frac{1}{2\pi}\ \omega_0 = \frac{1}{2\pi}\ \sqrt{\frac{K}{M}} = 10.99$ GHz is therefore obtained, as expected, as well as a normalized load participation factor Γ of 2.29 $\times 10^{18}$ kg^{-1}. The maximum von Mises stress factor in the sphere, yielding the maximum von Mises stress upon multiplication by $p(t)$, was also computed and turned out to be $t_{vM} = 1.21 \times 10^{17}$ Pa/m.

According to Lamb's theory [18], the eigenfrequency f_0 is inversely proportional to the particle radius R. Moreover, if material properties ($\mathbb{C}$, ρ_m) and overall charge (q) are independent of R, by (8) it follows that $K \sim R$, $M \sim R^3$, and $L \sim R^0$. Similarly, $t_{vM} \sim R^{-1}$. Those dependencies were verified numerically by running a Parametric Sweep on the virus radius in the [40, 60] nm range.

C. Frequency Response Analysis

According to (10), the transfer function from $f(t)$ to $p(t)$ is given by:

$$H\left(s\right) = \frac{\Gamma q \bar{E}}{s^2 + 2\zeta\omega_0 s + \omega_0^2}. \tag{13}$$

The Bode amplitude diagram of the von Mises stress $\sigma_{vM} = t_{vM}\ p$ is shown in Fig. 3, assuming unit field intensity $\bar{E}$ and overall charge $q = 1.16 \times 10^7 e$, reported in [11] for influenza A (H3N2) virus. Two different values of the damping factor ζ are considered, to mimic the response of the virus in air (panel A) or in water (panel B). Specifically, in the first case a low value $\zeta = \zeta_i = 0.02$ (corresponding to $Q = 25$) is set, which is associated to the intrinsic damping (ζ_i) of the viral particle. When the virus is in water, the overall damping factor ζ is given by the sum of the intrinsic damping factor ζ_i and the water-associated viscous contribution ζ_w. The latter is set to $\zeta_w = 0.125$ (corresponding to $Q = 4$) in agreement with [9], [12], [28]. The frequency responses obtained with the SDOF model (blue solid lines) are compared with those obtained with the FEM model – Frequency Domain study (green dashed lines), showing a very good agreement. As expected, the SDOF model successfully reproduces the resonance associated to the first dipolar mode (10.99 GHz), while missing the smaller resonance at 22.13 GHz, which is associated to the second dipolar mode. On a workstation with Intel(R) Xeon(R) CPU E5-2660 v3 @ 2.60GHz and 128 GB RAM, the computational time of the SDOF model was negligible, while the computational time of the FEM model was above 6 min per test.

It is noticed that airborne pathogens are typically transmitted via droplets or aerosols. Accordingly, the air model (Fig. 3(a)) serves primarily as a comparative benchmark, to highlight the influence of damping from the surrounding medium (Fig. 3(b)) or to approximate edge conditions such as nearly dry aerosols or surface exposure.

D. Population Study Via Monte Carlo Simulations

Leveraging its accuracy and computational effectiveness, the SDOF model was used to study the frequency response of a population of viruses, accounting for their heterogenous size. Following a Monte Carlo approach, a population of 20000 viruses with radii following a normal distribution with mean value $r = 50$ nm and 10% coefficient of variation [12], [29] was generated. The relevant coefficients of the SDOF model were obtained from those associated with the average radius by using the dependencies reported in Section IV-B: $f_0 \sim R^{-1}$, $K \sim R$, $M \sim R^3$, $L \sim R^0$, and $t_{vM} \sim R^{-1}$. The overall frequency response of the population in air is reported in Fig. 4(a). Considering the median behavior, the quality factor Q turned out to be 4.4, reproducing the experimentally observed broadening of the resonance range that is associated with heterogeneous virus size [12]. The addition of the water damping further

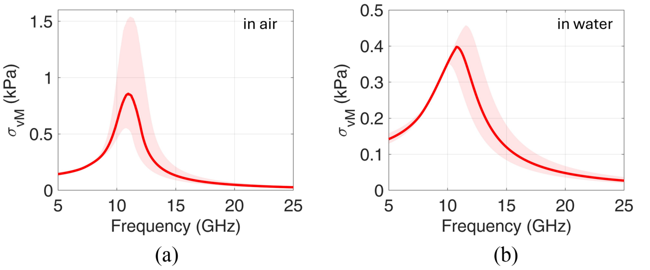

(a) (b)

Fig. 4. Frequency response of a population of viruses, (a) in air and (b) in water. The red line denotes the median response, while the shaded areas denote the interquartile range.

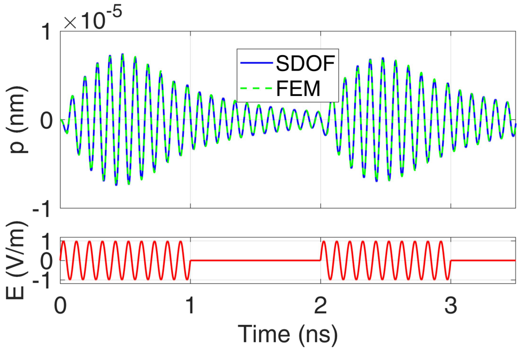

Fig. 5. Time domain analysis of the dipolar coupling, in case of harmonic electric field (10 GHz) modulated by a square wave (0.5 GHz). The relative vertical displacement between the poles and the center is reported, showing very good agreement between the SDOF model solution and the FEM model solution.

decreased the quality factor down to $Q = 2.4$ (Fig. 4(b)). The computational time of the Monte Carlo analysis was about 22 s. By comparison, the FEM frequency response analysis of 20000 samples would require almost 3 months.

In passing, hybrid approaches combining FEM simulations with machine learning have also been explored to address computational challenges. For instance, Mukhopadhyay et al. [17] trained a machine-learning model on FEM-generated data to efficiently perform Monte Carlo simulations.

E. Time-Domain Analysis

Besides the frequency response analysis, the SDOF model can be used to study the dipolar coupling between the virus and the applied electric field in the time domain, by solving (10) for $p(t)$. Several types of electrical stimulation ($\bar{E} f(t)$) can be easily addressed. As an example, Fig. 5 shows the case of harmonic stimulation at 10 GHz, modulated by a square wave at 0.5 GHz (in air medium). Since the frequency of the applied field (10 GHz) is close, but not equal, to the eigenfrequency of the first dipolar mode (10.99 GHz), a beat followed by an exponential decay is observed. For validation purposes, the solution $p(t)$ of the SDOF model is compared with the relative vertical displacement between the poles and the center of the sphere provided by the FEM model – Time Domain study. A very good agreement is found (the relative error in the L^2-norm is 4%). However, the computational time of the FEM model exceeds 10 minutes, whereas that of the SDOF model is negligible.

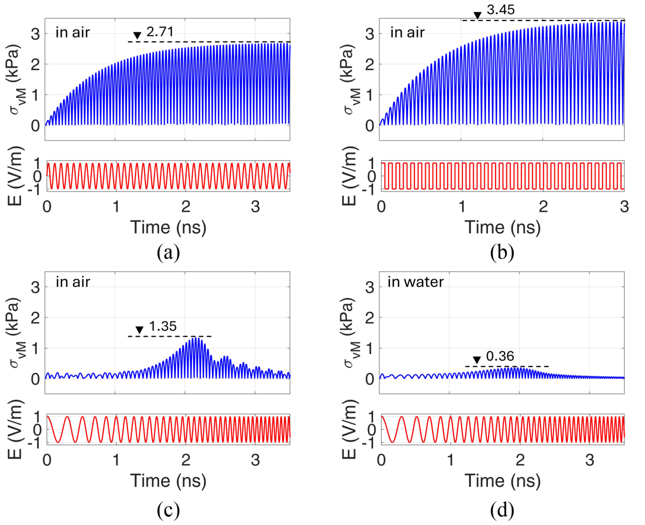

(a) (b)

(c) (d)

Fig. 6. Time domain analysis of the dipolar coupling (SDOF model, von Mises stress) in case of: (a) harmonic stimulation and (b) square wave stimulation, at 10.99 GHz (eigenfrequency of the first dipolar mode) in air; (c) and (d) chirp stimulation from 2.75 to 44 GHz, in air and water, respectively.

Additional examples are presented in Fig. 6. A harmonic stimulation with unit amplitude at the resonant frequency (10.99 GHz) induces rapidly growing oscillations that stabilize at a von Mises stress amplitude of 2.71 kPa (panel A). By comparison, a square wave stimulation with same amplitude and frequency elicits oscillations with a steady-state amplitude of 3.45 kPa (panel B). As expected, this value is $4/\pi$ times greater than the previous one, reflecting the amplitude of the square wave's fundamental harmonic. However, from an experimental standpoint, harmonic excitations are easier to generate and control, making them a more practical choice. Assuming a threshold stress to fracture the lipid envelope of 141 kPa [11], due to the linearity of the model, an applied electric field of about 54 V/m would be required. On the other hand, nanoscale fatigue could play a crucial role [20], reducing the stress threshold that leads to fracture, and accordingly the required electric field. By contrast, since the capsid of non-enveloped viruses is more resistant than the lipid membrane of enveloped viruses [2], higher electric fields may be needed for mechanical inactivation of non-enveloped viruses.

The case of a chirp stimulation with frequencies ranging from 2.75 to 44 GHz is shown in panel C (air medium) and panel D (water medium). As expected, a maximum response is found near the resonant frequency (10.99 GHz), with its amplitude strongly affected by the chirp duration and viscous damping.

V. DISCUSSION

By encapsulating a system's essential dynamic characteristics with a minimal number of parameters (mass, stiffness, damping), generalized SDOF models provide foundational understanding and enable quick, practical analysis of structures that would otherwise require more complex multi-degree-of-freedom models. This simplicity is particularly useful for preliminary design and identifying key dynamic behaviours.

The SDOF model developed in this work is based on the continuum hypothesis. While the accuracy of this approximation may decrease at scales near 50 nm, prior research supports this approach. For instance, Liu et al. [7] showed that treating a virus as an elastic sphere (Lamb's theory) can predict the dipolar resonance frequencies observed experimentally. Moreover, continuum-based modelling approaches were successfully used in several previous works (e.g., [8], [9], [11], [17], [19]). On the other hand, accounting for finer molecular effects calls for higher-resolution methods, at the expense of increased computational cost.

Modelling resonant dipolar coupling of viruses requires a few geometric and material parameters. Virus shape, size and envelope thickness can be measured with good accuracy with advanced microscopy techniques such as cryo-electron microscopy [30]. Virus density is approximately 1350 kg/m^3, reflecting their composition as a mixture of proteins (with densities near 1300 kg/m^3) and nucleic acids (around 1700 kg/m^3) [31]. On the other hand, mechanical properties like Young's modulus (Y) are not well established, with reported values that exhibit large variations depending on the measurement approach. In the present work, a Young's modulus of 3 GPa was used. This value results from the values assumed for the density (1350 kg/m^3) and for the sound velocities ($V_L = 1920$ m/s, $V_T/\ V_L = 1/2$) [25]. Other works that estimate the Young's modulus from atomic-force-microscopy indentation experiments report lower values. For instance, Nonn et al. [20] reported a Young's modulus on the order of tens of MPa. The proper estimation of particle mechanical properties is critical, since it affects the resonance frequency, which is proportional to the square root of Y.

Another property that requires further experimental investigation is the charge within the virus. In fact, charge amount and spatial distribution directly affect the force induced on the virus by microwave dipolar coupling, and therefore the estimated stress for a given applied electric field.

In the proposed SDOF model, the equivalent stiffness K is directly proportional to the Young's modulus Y, while the equivalent mass M scales with the mass density ρ_m. Consequently, the resonance frequency ($\omega_0 = \sqrt{K/M}$) is proportional to the square root of the ratio between the Young's modulus and the mass density, $\sqrt{Y/\rho_m}$. Additionally, the load participation factor L is influenced by the charge density ρ_c, assumed to be uniformly distributed throughout the shell and the core.

In constructing the SDOF model, we used the dipolar eigenmode corresponding to $n = 0$ (i.e., the lowest-frequency dipolar mode) as the shape function. The SDOF model could also be built by considering the second ($n = 1$) or third ($n = 2$) eigenmode as the shape function. However, those higher-order modes exhibit increasingly complex spatial profiles, with values alternating between positive and negative. This leads to progressively weaker coupling with the external driving force, whose spatial distribution is governed by core-shell charge separation. The reduced coupling of higher modes is confirmed by experimental evidence (cf., e.g., Fig. 2 of [7]) and by FEM analysis of frequency response (cf. Fig. 3(a), dashed line).

In the present work, our aim was to develop a general framework for modelling a spherical virus and to demonstrate the feasibility of the SDOF reduction. The model complexity could be further increased, for instance, to account for the virus's non-homogeneous structure. As a first step, we performed a parametric FEM-based free vibration analysis by varying either the shell or the core Young's modulus (cf. Figure S3 of the Supplementary Material). The results indicate that, while the effect of the shell's Young's modulus is quite modest, variations in the core's Young's modulus from 0.8 to 5.6 GPa lead to changes in the dipolar mode frequency ranging from 6.3 to 14 GHz. For any parameter set, the relevant displacement field of the first dipolar mode could serve as a shape function for developing the corresponding SDOF model. Additional features—such as nonlinear constitutive behavior, pre-stress due to osmotic pressure, constraints simulating the attachment to a host cell, or a non-uniform charge distribution across the core and the shell—could similarly be incorporated into the free vibration analysis to derive a corresponding shape function for the SDOF reduction. Nevertheless, this poses a challenge due to the limited availability of reliable estimates for viral material properties and charge distribution, which are scarcely documented in the current literature.

VI. CONCLUSION

We developed a generalized SDOF model for the investigation of viral inactivation via dipolar coupling under microwave irradiation. The proposed model uses the first dipolar mode as a shape function. Model parameters are derived from FEM-based free vibration analysis. While relying on a reduced-order representation, the model captures the key physical mechanisms underlying SRET and enables accurate prediction of viral response in both the frequency and time domains.

The generalized SDOF model demonstrates very good agreement with full 3D FEM simulations, while reducing computational costs by several orders of magnitude. It accurately reproduces the resonance behavior associated with the first dipolar mode and accounts for damping effects due to surrounding media, such as water. Moreover, it can be effectively applied to population studies via Monte Carlo simulations. The latter focused on virus radius to represent stochastic biological variability and captured the experimentally observed broadening of the resonance due to size heterogeneity. Uncertainty in Young's modulus, though significant, is epistemic and was addressed through parametric analysis, revealing that Young's modulus changes lead to substantial shifts in resonance frequency.

The model provides a versatile framework for interpreting experimental data and optimizing exposure protocols, and it can be extended to accommodate more complex viral morphologies and heterogeneous material properties. As a perspective, joint numerical and experimental activities are required to calibrate material parameters, damping factors, and charge distributions, thereby enhancing predictive reliability across viral species and environmental scenarios.

APPENDIX A
FEM MODEL

The FEM model was developed in COMSOL Multiphysics 6.2, with the Structural Mechanics Module. To reduce the computational time, a 15° sector of the sphere was studied, under cyclic-symmetry periodic conditions. The Solid Mechanics physics was used, with a Linear Elastic Material model. Material properties, namely, the shear modulus G and the bulk modulus B were computed from the following relationships [23]:

$$G = V_T^2\,\rho_m,\ B = V_L^2 \rho_m - \frac{4}{3}G, \tag{14}$$

assuming $V_L = 1920$ m/s, $V_T = V_L\,/2$, and $\rho_m = 1350$ kg/m^3. This density value is commonly used for viruses, which are a complex of proteins (density around 1300 kg/m^3) and nucleic acids (density around 1700 kg/m^3) [31]. Unless otherwise stated, a radius of 50 nm was assumed, which is typical of SARS-CoV-2 [24] and spherical forms of influenza viruses [32], and a shell thickness of 3.6 nm [30].

An Eigenfrequency study was set for the free vibration analysis. Specifically, the first 20 eigenfrequencies were determined and those relevant to the spherical eigenmodes were compared with the theoretical ones (Lamb's solution) for validation, achieving an excellent agreement ($\sim 10^{-5}$ relative difference). The solution corresponding to the first dipolar mode ($f_0 = 10.99$ GHz) was identified and used to compute the integral quantities in (8), which are required to implement the SDOF model, as well as the relevant maximum von Mises stress factor in the sphere (t_{vM}).

The FEM model was also used to investigate the interaction of the virus with an applied electric field, for comparison purposes with the SDOF model. Both the frequency response analysis (Frequency Domain study) and the transient response analysis (Time Domain study) were performed. For the transient response analysis, a null-average-w constraint was imposed, to prevent kinematic instability. The Rayleigh model was used to introduce damping in the FEM model (see e.g., [21]). Specifically, the mass-proportional and stiffness-proportional parameters of the Rayleigh model were computed by assigning the (same) damping factor ζ at two eigenfrequencies (i.e., the first torsional mode, 7.64 GHz, and the first dipolar mode, 10.99 GHz).

Hexahedral elements (quadratic serendipity) were used. Typical mesh sizes were 8400 elements for the Eigenfrequency study, and 1600 elements for the Frequency Domain and Time Domain studies.

DISCLOSURE

P. Bia, M. L. and A. M. are employees of Elettronica S.p.A. The remaining authors declare that they have no conflicts of interest related to this work.

REFERENCES

[1] L. Song et al., "Airborne pathogenic microorganisms and air cleaning technology development: A review," *J. Hazardous Mater.*, vol. 424, 2022, Art. no. 127429, doi: 10.1016/j.jhazmat.2021.127429.

[2] M. Sadraeian et al., "Virus inactivation by matching the vibrational resonance," *Appl. Phys. Rev.*, vol. 11, no. 2, 2024, Art. no. 021324, doi: 10.1063/5.0183276.

[3] B. W. Hoff et al., "Observed reductions in the infectivity of bioaerosols containing bovine coronavirus under repetitively pulsed RF exposure," *IEEE Trans. Biomed. Eng.*, vol. 70, no. 2, pp. 640–649, Feb. 2023, doi: 10.1109/TBME.2022.3199333.

[4] C. Wang, X. Hu, and Z. Zhang, "Airborne disinfection using microwave-based technology: Energy efficient and distinct inactivation mechanism compared with waterborne disinfection," *J. Aerosol Sci.*, vol. 137, 2019, Art. no. 105437, doi: 10.1016/j.jaerosci.2019.105437.

[5] J. Van Impe et al., "State of the art of nonthermal and thermal processing for inactivation of micro-organisms," *J. Appl. Microbiol.*, vol. 125, no. 1, pp. 16–35, 2018, doi: 10.1111/jam.13751.

[6] P. Wust et al., "Non-thermal effects of radiofrequency electromagnetic fields," *Sci. Rep.*, vol. 10, no. 1, 2020, Art. no. 13488, doi: 10.1038/s41598-020-69561-3.

[7] T. M. Liu et al., "Microwave resonant absorption of viruses through dipolar coupling with confined acoustic vibrations," *Appl. Phys. Lett.*, vol. 94, no. 4, 2009, Art. no. 043902, doi: 10.1063/1.3074371.

[8] C. K. Sun et al., "Resonant dipolar coupling of microwaves with confined acoustic vibrations in a rod-shaped virus," *Sci. Rep.*, vol. 7, no. 1, Dec. 2017, Art. no. 4611, doi: 10.1038/s41598-017-04089-7.

[9] T. M. Liu et al., "Effects of hydration levels on the bandwidth of microwave resonant absorption induced by confined acoustic vibrations," *Appl. Phys. Lett.*, vol. 95, no. 17, 2009, Art. no. 173702, doi: 10.1063/1.3254251.

[10] Y. Xiao, L. Zhao, and R. Peng, "Effects of electromagnetic waves on pathogenic viruses and relevant mechanisms: A review," *Virology J.*, vol. 19, no. 1, 2022, Art. no. 161, doi: 10.1186/s12985-022-01889-w.

[11] S. C. Yang et al., "Efficient structure resonance energy transfer from microwaves to confined acoustic vibrations in viruses," *Sci. Rep.*, vol. 5, Dec. 2015, Art. no. 18030, doi: 10.1038/srep18030.

[12] P. J. Wang et al., "Microwave resonant absorption of SARS-CoV-2 viruses," *Sci. Rep.*, vol. 12, no. 1, Dec. 2022, Art. no. 12596, doi: 10.1038/s41598-022-16845-5.

[13] A. Barbora and R. Minnes, "Targeted antiviral treatment using nonionizing radiation therapy for SARS-CoV-2 and viral pandemics preparedness: Technique, methods and practical notes for clinical application," *Plos One*, vol. 16, no. 5, May 2021, Art. no. e0251780, doi: 10.1371/journal.pone.0251780.

[14] P. Bia et al., "Selected microwave irradiation effectively inactivates airborne avian influenza A(H5N1) virus," *Sci. Rep.*, vol. 15, no. 1, 2025, Art. no. 2021, doi: 10.1038/s41598-025-85376-6.

[15] A. Manna et al., "Endemic respiratory viruses inactivation in aerosol by means of radiated microwaves," *Med. Res. Arch.*, vol. 11, no. 10, pp. 1–10, 2023, doi: 10.18103/mra.v11i10.4486.

[16] A. Manna et al., "SARS-CoV-2 inactivation in aerosol by means of radiated microwaves," *Viruses*, vol. 15, no. 7, Jul. 2023, Art. no. 1443, doi: 10.3390/v15071443.

[17] T. Mukhopadhyay et al., "Probing the stochastic dynamics of coronaviruses: Machine learning assisted deep computational insights with exploitable dimensions," *Adv. Theory Simul.*, vol. 4, no. 7, Jul. 2021, Art. no. 2000291, doi: 10.1002/adts.202000291.

[18] H. Lamb, "On the vibrations of an elastic sphere," *Proc. London Math. Soc.*, vol. s1–13, no. 1, pp. 189–212, 1881, doi: 10.1112/plms/s1-13.1.189.

[19] C. Warsame et al., "Modal analysis of novel coronavirus (SARS COV-2) using finite element methodology," *J. Mech. Behav. Biomed. Mater.*, vol. 135, Nov. 2022, Art. no. 105406, doi: 10.1016/j.jmbbm.2022.105406.

[20] A. Nonn et al., "Inferring mechanical properties of the SARS-CoV-2 virus particle with nano-indentation tests and numerical simulations," *J. Mech. Behav. Biomed. Mater.*, vol. 148, Dec. 2023, Art. no. 106153, doi: 10.1016/j.jmbbm.2023.106153.

[21] A. Chopra, *Dynamics of Structures: Theory and Applications to Earthquake Engineering*, Pearson College Div, 2016.

[22] G. J. Taylor, J. Margueritat, and L. Saviot, "Comment on manna et al. SARS-CoV-2 inactivation in aerosol by means of radiated microwaves," *Viruses*, vol. 15, 2023, Art. no. 2110, doi: 10.3390/v15102110.

[23] M. E. Gurtin, "The linear theory of elasticity," in *Linear Theories of Elasticity and Thermoelasticity*, C. Truesdell, Ed., Berlin, Germany: Springer-Verlag, 1973, pp. 1–295, doi: 10.1007/978-3-662-39776-3_1.

[24] N. Zhu et al., "A novel coronavirus from patients with pneumonia in China, 2019," *New England J. Med.*, vol. 382, no. 8, pp. 727–733, Feb. 2020, doi: 10.1056/nejmoa2001017.

[25] B. Stephanidis et al., “Elastic properties of viruses,” *Biophys. J.*, vol. 93, no. 4, pp. 1354–1359, 2007, doi: 10.1529/biophysj.107.109033.

[26] J. Miklowitz, *The Theory of Elastic Waves and Waveguides* (North-Holland series in Applied Mathematics and Mechanics), vol. 22, North-Holland: Amsterdam, 1994.

[27] K. F. Graff, *Wave Motion in Elastic Solids*. New York, NY, USA: Dover Publications, 1991.

[28] V. A. Fonoberov and A. A. Balandin, “Low-frequency vibrational modes of viruses used for nanoelectronic self-assemblies,” *Phys. Status Solidi B Basic Res.*, vol. 241, no. 12, pp. R67–R69, Oct. 2004, doi: 10.1002/pssb.200409062.

[29] M. Laue et al., “Morphometry of SARS-CoV and SARS-CoV-2 particles in ultrathin plastic sections of infected Vero cell cultures,” *Sci. Rep.*, vol. 11, no. 1, Dec. 2021, Art. no. 3515, doi: 10.1038/s41598-021-82852-7.

[30] S. Klein et al., “SARS-CoV-2 structure and replication characterized by in situ cryo-electron tomography,” *Nature Commun.*, vol. 11, no. 1, Dec. 2020, Art. no. 5885, doi: 10.1038/s41467-020-19619-7.

[31] H. M. Mazzone, *CRC Handbook of Viruses: Mass-Molecular Weight Values and Related Properties*, Boca Raton, FL, USA: CRC Press, 1998.

[32] N. M. Bouvier and P. Palese, “The biology of influenza viruses,” *Vaccine*, vol. 26, no. 4, pp. D49–D53, 2008, doi: 10.1016/j.vaccine.2008.07.039.